Reduced entropic model for studies of multidimensional nonlocal transport in high-energy-density plasmas

D. Del Sorbo, J.-L. Feugeas, Ph. Nicolaï, M. Olazabal-Loumé, B. Dubroca, S. Guisset, M. Touati, and V. Tikhonchuk

Citation: Phys. Plasmas **22**, 082706 (2015); doi: 10.1063/1.4926824
View online: http://dx.doi.org/10.1063/1.4926824
View Table of Contents: http://aip.scitation.org/toc/php/22/8
Published by the American Institute of Physics

Reduced entropic model for studies of multidimensional nonlocal transport in high-energy-density plasmas

D. Del Sorbo, J.-L. Feugeas, Ph. Nicolaï, M. Olazabal-Loumé, B. Dubroca, S. Guisset, M. Touati, and V. Tikhonchuk
Centre Lasers Intenses et Applications, Université de Bordeaux-CNRS-CEA, UMR 5107, F-33405 Talence, France

(Received 2 March 2015; accepted 1 July 2015; published online 12 August 2015)

Hydrodynamic simulations of high-energy-density plasmas require a detailed description of energy fluxes. For low and intermediate atomic number materials, the leading mechanism is the electron transport, which may be a nonlocal phenomenon requiring a kinetic modeling. In this paper, we present and test the results of a nonlocal model based on the first angular moments of a simplified Fokker-Planck equation. This multidimensional model is closed thanks to an entropic relation (the Boltzman H-theorem). It provides a better description of the electron distribution function, thus enabling studies of small scale kinetic effects within the hydrodynamic framework. Examples of instabilities of electron plasma and ion-acoustic waves, driven by the heat flux, are presented and compared with the classical formula. © *2015 AIP Publishing LLC*.
[http://dx.doi.org/10.1063/1.4926824]

I. INTRODUCTION

High-energy-density plasmas are created in the interaction of intense laser beams with solid targets. In particular, in Inertial Confinement Fusion (ICF), nanosecond laser pulses are used to implode and ignite a deuterium-tritium target. Laser pulses cannot penetrate deeply into the matter and the laser energy is deposited in a low density plasma, below the electron critical density $n_c = 1.1 \times 10^{21} \lambda_L^{-2} \mathrm{cm}^{-3}$, where λ_L is the laser wavelength in μm. The deposited energy is transported to the denser part of target by the electron conduction. The ablation rate, the pressure, and the implosion velocity depend on this energy transfer.[1] Although the electron heat transport plays a key role, it is not correctly modeled in large ICF numerical tools. Indeed, the electron conduction model implemented in the majority of codes is based on the Spitzer and Härm[2] (SH) theory. But, if the electron mean free path (MFP) exceeds about 2×10^{-3} times the temperature gradient length, the SH theory is no more valid and a nonlocal model is needed.[3] This is a common case in the ICF context.

Various macroscopic nonlocal models have been proposed,[4–6] improved,[7,8] and compared.[9,10] However, most of them are not adapted for being used in hydrodynamic codes, especially in a multidimensional geometry. The only exception is the one proposed by Schurtz, Nicolaï, and Busquet[11–13] (SNB), based on the multi-group transport scheme. In the SNB model, nonlocal effects are computed by finding at each temporal step the energy distribution of fast electrons, from a stationary and simplified Fokker-Planck (FP) equation, assuming a weak anisotropy and a small deviation from equilibrium of the suprathermal part of the electron distribution function (EDF). In this model, the electric and magnetic field effects on suprathermal electrons are taken into account through phenomenological corrections.[14] These corrections can be very complex and numerically unstable, especially in the case where the magnetic fields are present.

In ICF targets, strong magnetic fields are generated all over the conduction zone, but can also be excited inside the imploding target, induced by nonlocal effects.[15] Although these fields may strongly modify the heat transport, a simple and self-consistent electromagnetic nonlocal transport theory, which can be coupled with hydrodynamic codes, is still missing.

We develop here a nonlocal kinetic model based on angular interpolation of the FP equation, closed by the angular entropy maximization.[16] This model, called M1 (Ref. 17) for the first angular moment, has already been tested for the relativistic electron beam transport through matter,[18] in domains of fast ignition and medical applications. However, such a model cannot be applied for studies for nonlocal transport as the fast electrons are considered as separate species, and not as a part of the overall electron distribution function. In this paper, we develop a modified M1 model, allowing nonlocal transport calculations and taking advantage of the entropic closure. We show that the entropic closure allows an extension of the domain of application to stronger anisotropic cases, while the advective form of equations leads to an easier accounting for electromagnetic fields.

In this paper, we develop the M1 model in the domain of nonlocal transport, presenting several examples in 1D and 2D geometry and analyzing the small scale kinetic effects in the transport affected zone. In particular, we introduce a simplified version of the FP equation in Section II, and our model as well as the SNB model in Section III. In Section IV we compare these models in ICF conditions, and in Section V we discuss modifications of damping of electrostatic plasma waves and excitation of stream instabilities in the transport zone. Conclusions are drawn in Section VI.

II. TRANSPORT AND COLLISIONS

The heat flux is defined as the energy transported from a hot region to a cold one over unit time and unit surface

$$\vec{q} = \langle n_e \epsilon \vec{v} \rangle = \int_{\mathbf{R}^3} d^3 v \epsilon \vec{v} f_e, \tag{1}$$

where ϵ is the electron kinetic energy and $f_e = f_e(\vec{x}, \vec{v}, t)$ is the phase space EDF, which depends on the space $\vec{x}$, the velocity $\vec{v}$, and the time t. The integration is performed over the 3-dimensional real space $\mathbf{R}$. In what follows, m_e, e, and c refer, respectively, to the electron mass, the elementary charge, and the speed of light, T_e and n_e refer to the electron temperature and density, and $\vec{E}$ and $\vec{B}$ refer to the electric and magnetic fields.

In case of binary and small angle collisions (classical plasmas), the EDF evolution is given by the FP equation

$$\left(\frac{\partial}{\partial t} + \vec{v} \cdot \vec{\nabla} + \frac{\vec{F}}{m_e} \cdot \vec{\nabla}_v \right) f_e = \left(\frac{\partial f_e}{\partial t} \right)_{\text{coll}}, \tag{2}$$

which takes into account both collective and collisional effects. The symbol $\vec{\nabla}_v$ means gradient respect to the velocity vector. The collective effects are described by the Lorentz force $\vec{F} = -e(\vec{E} + \frac{\vec{v}}{c} \times \vec{B})$, and the right hand side is the Landau collision term.[19] Assuming that the plasma is composed by electrons (subscript e) and one ion species (subscript i), the full Landau collision term reads

$$\left(\frac{\partial f_e}{\partial t} \right)_{\text{coll}} = \sum_{j=e,i} \frac{\partial}{\partial \vec{p}_e} \int_{\mathbf{R}^3} d^3 v_j \bar{\bar{U}} \left(\frac{\partial f_e}{\partial \vec{p}_e} f_j - \frac{\partial f_j}{\partial \vec{p}_j} f_e \right), \tag{3}$$

with

$$\bar{\bar{U}} = \frac{U_0}{2} \frac{u^2 \bar{\bar{I}} - \vec{u} \otimes \vec{u}}{u^2},$$

$\vec{u} = \vec{v}_e - \vec{v}_j$ as the relative velocity and

$$U_0 = \frac{4\pi e^2 q_j^2 \Lambda_{ej}}{u}$$

as the scattering potential. The symbols m_j, q_j, and p_j refer, respectively, to the mass, the charge, and the momentum of a particle j, while Λ_{ej} refers to the Coulomb logarithm for electrons colliding with j-particles.

The Landau collision operator is complicated and too much time-consuming to be solved with a hydrodynamic code. The simplifications are as follows: the ions are supposed to have infinite mass and their velocity is neglected. Target electrons are supposed at the equilibrium and their deviation from equilibrium is induced by suprathermal electrons. Then, the collision term in Eq. (3) reads[20,21]

$$\left(\frac{\partial f_e}{\partial t} \right)_{\text{coll}} = S_{ee} \frac{\partial}{\partial p} \left(\frac{v_{th}^2}{v} \frac{\partial}{\partial v} + 1 \right) (f_e - f^m) + \frac{\nu_{ee} + \nu_{ei}}{2} \frac{\partial^2}{\partial \vec{\Omega}^2} f_e, \tag{4}$$

where $S_{\alpha\beta} = \nu_{\alpha\beta} p_\alpha m_\alpha / m_\beta$ is the classical stopping power, $\nu_{\alpha\beta} = \frac{4\pi n_\beta q_\alpha^2 q_\beta^2 \Lambda_{\alpha\beta}}{m_\alpha^2 v_\alpha^3}$ is the collision frequency, $v_{th} = \sqrt{T_e / m_e}$ is the thermal velocity, $f^m = n_e / (2\pi v_{th})^{3/2} e^{-v^2/(2v_{th}^2)}$ is the Maxwellian EDF, and

$$\frac{\partial^2}{\partial \vec{\Omega}^2} = \frac{1}{\sin\theta} \frac{\partial}{\partial \theta} \left(\sin\theta \frac{\partial}{\partial \theta} \right) + \frac{1}{\sin^2\theta} \frac{\partial^2}{\partial \phi^2}$$

is the Laplace-Beltrami operator. Here, θ and ϕ are the velocity angles, in spherical coordinates. The term containing the Maxwellian EDF is important for the theory of nonlocal transport as it allows to join the fast electron distribution with the local population of thermal electrons.

As the heat is transported by suprathermal electrons, the first term in the right hand side of Eq. (4) can be simplified by retaining only the friction term and neglecting the diffusion one. This simplification is only valid for the fast electrons, it conserves the number of particles and describes the relaxation to the equilibrium Maxwellian distribution. The suprathermal assumption ($v_{th}^2 / v^2 \ll 1$) leads to

$$\left(\frac{\partial f_e}{\partial t} \right)_{\text{coll}} = \nu_{ee} v \frac{\partial}{\partial v} (f_e - f_e^m) + \frac{\nu_{ee} + \nu_{ei}}{2} \frac{\partial^2}{\partial \vec{\Omega}^2} f_e. \tag{5}$$

The electron-electron collision term corresponds to the collision operator derived by Albritton, Williams, Bernstein and Swartz[22] (AWBS).

III. REDUCED MODELS

Equation (2), with the collision operator in Eq. (5), is still computationally demanding and cannot be solved for each time step of a hydrodynamic code. A possible way to reduce the number of unknowns is to integrate over angles.[23] The angular moments of the EDF are defined as

$$\bar{\bar{f}}_l(\vec{x}, v, t) = \int_{S_2} d^2\Omega f_e(\vec{x}, \vec{v}, t) \underbrace{\otimes \vec{\Omega}}_{l-\text{times}},$$

where $\vec{\Omega}$ is the velocity direction vector, the double bar stands for tensor of generic order (higher than one) and $\otimes$ is the tensorial product. The integration is performed over the unitary sphere S_2 ($0 \le \theta \le \pi$, $0 \le \phi \le 2\pi$). Hence, the first three moments ($l = 0$, 1, and 2) read

$$\begin{cases} f_0 = \int_{S_2} d^2\Omega f_e \\ \vec{f}_1 = \int_{S_2} d^2\Omega f_e \vec{\Omega} \\ \bar{\bar{f}}_2 = \int_{S_2} d^2\Omega f_e \vec{\Omega} \otimes \vec{\Omega}. \end{cases} \tag{6}$$

In the same way, the first two moments of Eq. (2) read

$$\begin{cases} \dfrac{\partial f_0}{\partial t} + v \vec{\nabla} \cdot \vec{f}_1 - \dfrac{e\vec{E}}{m_e v^2} \cdot \dfrac{\partial}{\partial v} \left(v^2 \vec{f}_1 \right) = \left(\dfrac{\partial f_0}{\partial t} \right)_{\text{coll}} \\ \dfrac{\partial \vec{f}_1}{\partial t} + v \vec{\nabla} \cdot \bar{\bar{f}}_2 - \dfrac{e}{m_e v^2} \dfrac{\partial}{\partial v} \left(v^2 \bar{\bar{f}}_2 \cdot \vec{E} \right) + \dfrac{e}{m_e v} \left(f_0 \bar{\bar{I}} - \bar{\bar{f}}_2 \right) \cdot \vec{E} + \dfrac{e}{m_e c} \vec{f}_1 \times \vec{B} = \left(\dfrac{\partial \vec{f}_1}{\partial t} \right)_{\text{coll}}, \end{cases} \tag{7}$$

where $\bar{\bar{I}}$ is the second order identity tensor and the moment integrated collision operators read

$$\begin{cases} \left(\dfrac{\partial f_0}{\partial t}\right)_{\text{coll}} = \nu_{ee} v \dfrac{\partial}{\partial v}\left(f_0 - f_0^m\right) \\ \left(\dfrac{\partial \vec{f}_1}{\partial t}\right)_{\text{coll}} = \nu_{ee} v \dfrac{\partial}{\partial v}\vec{f}_1 - (\nu_{ee} + \nu_{ei})\vec{f}_1. \end{cases}$$

Magnetic fields are naturally taken into account as shown in Eq. (7). However, in what follows we will consider only unmagnetized plasmas, $\vec{B} = 0$.

As the electron collision time is much smaller than the hydrodynamic time scale, we can assume a quasi-stationary EDF, allowing to neglect the temporal derivatives. This level of approximation is compatible with hydrodynamic computations. However, the system (7) needs to be closed and the second moment needs to be given explicitly. The choice of this closure relation characterizes the model. We consider two closure relations, called, respectively, P1 and M1.

A. Polynomial closure

The system (7) can be closed by the assumption of small velocity anisotropies. Under this hypothesis, the EDF can be described by the first order development of the Cartesian tensor scalar product expansion (P1 approximation)

$$f_e(\vec{x}, \vec{v}, t) = \frac{f_0}{4\pi} + \frac{3\vec{\Omega} \cdot \vec{f}_1}{4\pi}. \tag{8}$$

With the moment definitions (6), Eq. (8) leads to the closure relation

$$\bar{\bar{f}}_2 = \frac{f_0}{3}\bar{\bar{I}}. \tag{9}$$

The relation (8) is simple and linear but it is valid only for weak anisotropies ($||\vec{f}_1|| \ll f_0$), which is not always fulfilled in the ICF conditions. In case of strong anisotropies, the P1 model can produce negative values for some electron energy groups, although the energy integration for the flux calculation may hide this unphysical behavior.

B. Entropic closure

The M1 model was developed in order to provide access to strongly anisotropic distributions.[17,18,24]

According to the second law of thermodynamics, all closed systems tend toward the thermal equilibrium. This behavior is expressed by the entropy maximization principle. The latter is exploited in the M1 model, over the angular directions. For each energy group, the local angular entropy reads

$$H_v[f_e] = -\int_{S_2} d^2\Omega (f_e \log f_e - f_e). \tag{10}$$

It is maximized with the constraint of the first two moment definitions (6). The Lagrangian of this maximization problem is

$$L[f_e] = H_v[f_e] - \alpha_0\left(f_0 - \int_{S_2} d^2\Omega f_e\right) - \vec{\alpha}_1 \cdot \left(\vec{f}_1 - \int_{S_2} d^2\Omega \vec{\Omega} f_e\right),$$

where α_0 and $\vec{\alpha}_1$ are two Lagrangian multipliers, which can be written as functions of f_0 and $\vec{f}_1$. The underlying M1 EDF maximizes the Lagrangian functional

$$\frac{d}{df_e} L[f_e] = 0 \Rightarrow f_e = N e^{\alpha_0 + \vec{\alpha}_1 \cdot \vec{\Omega}}, \tag{11}$$

where N is a normalization constant. The advantage of using this closure relation is that the underlying EDF is an exponential function. Thus, it is necessarily positively defined.

According to the definition (6) and using the underlying M1 EDF (11), we obtain the expressions for the angular moments

$$\begin{cases} f_0 = 4\pi N \dfrac{\sinh|\vec{\alpha}_1|}{|\vec{\alpha}_1|} e^{\alpha_0} \\ \vec{\Omega}_v = \dfrac{\vec{f}_1}{f_0} = \left(\coth|\vec{\alpha}_1| - \dfrac{1}{|\vec{\alpha}_1|}\right) \dfrac{\vec{\alpha}_1}{|\vec{\alpha}_1|}, \end{cases} \tag{12}$$

where $\vec{\Omega}_v$ is the anisotropy vector, such that $0 \leq ||\vec{\Omega}_v|| \leq 1$. The inversion of the second equation in (12) provides the expression of the coefficient $\vec{\alpha}_1$ and hence the total EDF in function of the first two angular moments. Although, this inversion cannot be performed analytically, it was performed numerically and tabulated in Ref. 17 This expression can be interpolated analytically with a precision better than 5% as

$$\vec{\alpha}_1 \approx \frac{3\vec{\Omega}_v}{1 - \frac{\vec{\Omega}_v^2}{2}\left(1 + \vec{\Omega}_v^2\right)}. \tag{13}$$

Then, the total EDF takes the following form:

$$f_e = f_0 \frac{|\vec{\alpha}_1|}{4\pi \sinh|\vec{\alpha}_1|} e^{\vec{\alpha}_1 \cdot \vec{\Omega}}. \tag{14}$$

Using the moment definitions, we can find the closure relation

$$\bar{\bar{f}}_2 = \bar{\bar{\chi}}(f_0, \vec{f}_1) f_0, \tag{15}$$

with

$$\bar{\bar{\chi}}\left(f_0, \vec{f}_1\right) = \frac{1}{3}\bar{\bar{I}} + \mu\left(\frac{\vec{f}_1 \otimes \vec{f}_1}{\vec{f}_1^{\,2}} - \frac{1}{3}\bar{\bar{I}}\right).$$

In Section IV, we present examples of recovering the total EDF from the first two angular moments according to Eqs. (13) and (14).

The advantage of the M1 models is in their capacity to describe strongly anisotropic systems. However, their implementation depends also on the considered physical processes. Specifically, in this paper, the form of collisional operators is chosen to describe the heat transfer and the thermalization of hot electrons. This is different from previous schemes[18] dedicated to the transport of relativistic electrons

which do not conserve the number of electrons and do not account for their thermalization. In the nonlocal flux context, these issues are of primary importance.

C. Diffusive nonlocal transport models

In the SH classical theory,[2] the EDF in Eq. (8) is assumed to be close to the equilibrium ($f_0 \approx f_0^m$). This corresponds to the hydrodynamic regime where the plasma is collisional and the MFP is small compared to the electron temperature gradient length. Thus, the first equation of the system (7) is not used anymore and only the second equation has to be solved.

The analytical solution for the electron transport coefficient can be found in the Lorentz gas approximation ($Z \gg 1$), for stationary and unmagnetized plasmas, and using the P1 closure relation.[2] Then, the second equation in (7) reads

$$\frac{v}{3}\vec{\nabla} f_0 - \frac{e\vec{E}}{3m_e}\frac{\partial}{\partial v} f_0 = -\nu_{ei}\vec{f}_1.$$

The electric field in this equation can be found from the requirement that the electric current

$$\vec{j}_e = -e\int_0^\infty dv v^3 \vec{f}_1$$

is equal to zero. Then, one obtains the following expression for the electric field:

$$\vec{E} = -\frac{m_e}{6e}\frac{\int_0^\infty \vec{\nabla} f_0 v^7 dv}{\int_0^\infty f_0 v^5 dv}, \tag{16}$$

which, along with the equilibrium assumption for f_0, reads

$$\vec{E}_{SH} = -\frac{T_e}{e}\left(\frac{\vec{\nabla} n_e}{n_e} + \xi\frac{\vec{\nabla} T_e}{T_e}\right). \tag{17}$$

Here, the coefficient $\xi = 2.5$ is in the limit $Z \gg 1$. There is no explicit analytical expression for the electric field if one is taking into account electron-electron collisions in Eq. (7). However, the expression (17) for the electric field is still a good approximation if the coefficient ξ is interpolated by the following expression: $\xi(Z) = 1 + 3/2(Z + 0.477)/(Z + 2.15)$. Knowing the electric field, one can also find an approximate expression for the first EDF moment

$$\vec{f}_1^m = -\frac{\lambda_{ei}^*}{3}\left(\frac{m_e v^2}{2T_e} - 4\right) f_0^m \frac{\vec{\nabla} T_e}{T_e}, \tag{18}$$

where λ_{ei}^* accounts for the ion charge Z dependence of the effective MFP

$$\lambda_{ei}^* = \frac{Z + 0.24}{Z + 4.2}\lambda_{ei}.$$

According to Eq. (1), the expression for the local SH heat flux reads

$$\vec{q}_{SH} = -k(T_e)\vec{\nabla} T_e,$$

with

$$k(T_e) = 0.4\frac{Z}{Z + 0.2\log(Z) + 3.44}\frac{20(2/\pi)^{3/2}T_e^{5/2}}{m_e^{1/2}e^4 Z\Lambda_{ei}}.$$

According to Eq. (18), the energy is mostly transported by suprathermal electrons having the velocity 3.7 times the thermal velocity.[11] Since the MFP varies as v^4, these electrons have a MFP 187 times higher than the thermal MFP. They can penetrate deeply in plasma and deposit their energy far from the point where they are originated. If the MFP of these electrons becomes comparable to the temperature gradient length ($\lambda_e > 2 \times 10^{-3} L_T$), the local theory is no more valid and nonlocal corrections are needed.

The most successful nonlocal model proposed so far is the multidimensional SNB model.[11] We remind in what follows its main assumptions. The SNB model accounts for deviations of the isotropic part of EDF from the Maxwellian distribution. It is based on Eq. (7), in the diffusive approximation and with a simplified Z-fitted Bhatnagar, Gross, and Krook (BGK) collisional operator[25]

$$\begin{cases} \left(\frac{\partial f_0}{\partial t}\right)_{\text{coll}} = -\nu_{ee}(f_0 - f_0^m) \\ \left(\frac{\partial \vec{f}_1}{\partial t}\right)_{\text{coll}} = -\nu_{ei}^* \vec{f}_1, \end{cases}$$

which is solved in a multi-group approximation neglecting the particle exchange between the energy groups. The main assumption of this model is splitting of the EDF in a local part, which leads to the SH flux, and a nonlocal one induced by suprathermal electrons, which leads to nonlocal effects. The isotropic part of EDF in the SNB approximation reads $f_0 = f_0^m + \Delta f_0$ and the anisotropic part $\vec{f}_1 = \vec{f}_1^m + \Delta\vec{f}_1$. Solving the first two moment equations, with the P1 closure, one finds a diffusion equation for the suprathermal electrons. It reads

$$\begin{cases} \left(\frac{1}{\lambda_{ee}} - \vec{\nabla}\frac{\lambda_{ei}^E}{3}\vec{\nabla}\right)\Delta f_0 = -\vec{\nabla}\vec{g}_1^m \\ \Delta\vec{f}_1 = -\frac{\lambda_{ei}^*}{3}\vec{\nabla}\Delta f_0, \end{cases}$$

where the source term $\vec{g}_1^m = -\frac{\lambda_{ei}^*}{3} f_0^m \frac{\vec{\nabla} T_e}{T_e}$ is a simplified form of Eq. (18), neglecting the return current, and $\lambda_{\alpha\beta} = v/2\nu_{\alpha\beta}$ is the effective collisional stopping length (see formula (23) in Ref. 11). The electric field in the SNB model is calculated according to the SH formula (17). Its effect on the electron transport is empirically taken into account for each energy group through a reduction of the electron-ion MFP to a physical stopping length $\frac{1}{\lambda_{ei}^E} = \frac{1}{\lambda_{ei}} + \frac{|e\vec{E}_{SH}|}{\epsilon}$. The nonlocal correction of the heat flux is given by $\Delta\vec{f}_1$

$$\vec{q}_{NL} = 2\pi m_e \int_0^\infty (\vec{f}_1^m + \Delta\vec{f}_1) v^5 dv = \vec{q}_{SH} + \Delta\vec{q}.$$

Although this model is computationally efficient and operates in three spatial directions, it cannot describe strong

deviations from the Maxwellian distribution and cannot easily account for the magnetic fields. This model is called BGK-SNB, along the paper.

In this paper, we improve the SNB model by replacing the BGK collisional term with the AWBS one.[5] This operator allows diffusion within energy groups and it is closer to the one used in P1 and M1 models. The improved model is deduced in the same way as BGK-SNB model, but with the new collision operator

$$\begin{cases} \left(\dfrac{\partial f_0}{\partial t}\right)_{\text{coll}} = \nu_{ee} v \dfrac{\partial}{\partial v}\left(f_0 - f_0^m\right) \\ \left(\dfrac{\partial \vec{f}_1}{\partial t}\right)_{\text{coll}} = -\nu_{ei}^* \vec{f}_1. \end{cases}$$

Then, the diffusion equation for the correction to the isotropic part of EDF reads

$$\left(\frac{v}{\lambda_{ee}}\frac{\partial}{\partial v} + \vec{\nabla}\frac{\lambda_{ei}^E}{3}\vec{\nabla}\right)\Delta f_0 = \vec{\nabla}\vec{g}_1^m.$$

In this equation, we use the standard kinetic definition of the MFP $\lambda_{\alpha\beta} = v/\nu_{\alpha\beta}$. This modified model is called AWBS-SNB along the paper.

IV. ELECTRON TRANSPORT

In this section, we compare the modified nonlocal models (M1, P1, and AWBS-SNB) with the BGK-SNB model, in several representative cases of heat transport.

In particular, the M1 and P1 computations are performed as follows.

- The initialization is given by hydrodynamic quantities (temperature and density), which can be computed at each temporal step of a hydrodynamic simulation. These quantities define the Maxwellian EDF f^m, which is used by collision operators. As a first guess, the electric field is assumed to depend on the hydrodynamic quantities, according to Eq. (17).
- The system (7) is closed with Eq. (9) or (15), respectively, in the P1 and M1 model. In this way, it is reduced to two equations for two unknowns (f_0 and $\vec{f}_1$). We solve it in the stationary limit, neglecting temporal derivatives. It is done for each velocity group v, from the highest to the lowest value and imposing $f_0(\vec{x}, v = v_{max}) = \vec{f}_1(\vec{x}, v = v_{max}) = 0, \forall \vec{x}$ and for a sufficiently high maximum velocity v_{max}.
- The deduced f_0 and $\vec{f}_1$ are used in Eq. (16), for the calculation of the nonlocal electric field. Since the validity of this formula is limited to Lorentz gases, we multiplied it by the factor $\xi/2.5$, as in Eq. (17). This fit is valid in the limit $\vec{\nabla}T_e/T_e \gg \vec{\nabla}n_e/n_e$, which is always respected in this paper. In the extreme case of $Z = 1$ and $\vec{\nabla}T_e/T_e \ll \vec{\nabla}n_e/n_e$, the error committed is ∼30%, smaller than in the codes which assume local electric fields. An equivalent choice could be to use Eq. (17), with hydrodynamic quantities, derived from the computed f_0. The new electric field is injected in the system (7), for a new iteration. This process is repeated till the zero current condition. Usually, it is achieved with the precision of a few percent after 2–3 iterations. This can be explained by the fact that the return current is carried out by slower electrons, which are more collisional and less sensitive to the nonlocal effects.
- Once the zero current condition is achieved, we compute hydrodynamic quantities from f_0 and $\vec{f}_1$. From f_0, we deduce the new temperature and density, which are close to the quantities given as initialization. This justifies the stationary assumption. According to Eq. (1), the heat flux is deduced from $\vec{f}_1$. The total EDF can be obtained from f_0 and $\vec{f}_1$. In the P1 model, it is given by Eq. (8), in the M1 model by Eqs. (13) and (14).

A temporal evolution of hydrodynamic quantities is calculated with a hydrodynamic code. The M1 as well as the P1 model should be computed in their (kinetic) stationary limit, at each hydrodynamic temporal step. The heat flux derived from these models is used in the subsequent hydrodynamic step. However, this paper is limited to a stationary analysis.

A. Transport along the temperature gradient

This case has already been considered for testing nonlocal models.[11] Let us consider a fully ionized Beryllium plasma at a constant density of $4.472 \times 10^{22}\,\text{cm}^{-3}$, having a steep temperature gradient given by

$$T_e(x) = \frac{|T_0 - T_1|}{2}\left[\frac{2}{\pi}\arctan\left(\frac{x}{\delta_{NL}}\right) + 1\right] + T_1, \qquad (19)$$

with $T_0 = 5\,\text{keV}$, $T_1 = 1\,\text{keV}$, and $\delta_{NL} = 5\,\mu\text{m}$.

It is helpful for the comprehension of the P1 and M1 models to detail the progression of the computation. The temperature in Eq. (19), with the constant density, initializes the models. The first-iteration electric field is given by Eq. (17). The system (7) is solved, as described above. The solution is iterated till to reach the zero current condition. From computed f_0 and $\vec{f}_1$, we deduce heat fluxes and total EDFs.

Heat fluxes computed with the previously described models are compared in Fig. 1(a). The fluxes are normalized to the maximum value of the local flux q_0 and the space is measured with the standard thermal MFP $\lambda_0 = 3\sqrt{\frac{\pi}{2}}\frac{T_0^2}{4\pi n_e Z e^4 \Lambda_{ei}}$ $\approx 3.15\,\mu\text{m}$. The nonlocal models show two main effects: a flux limitation (FL) and a preheat in the front of the temperature gradient. The former effect could be described by roughly limiting the SH flux to a fraction of the free streaming (FS) flux $q_{FS} = m_e n_e v_{th}^3$. However, this flux limitation (FL) model is not describing the preheat; moreover, the maximum of the heat flux is shifted to the high temperature zone.

All considered nonlocal models agree in the description of the heat flux. After velocity integration, no differences can be seen between P1 and M1 models, so we show only the latter. The flux limitation is different for each model and in the hot region we see that SNB models delocalize slightly more than M1.

Local and nonlocal electric fields are shown in Fig. 1(b). While smaller, there still is a difference between local and nonlocal electric fields. The curves M1 and P1 correspond to the same set of equations for f_0 and $\vec{f}_1$ but with the different

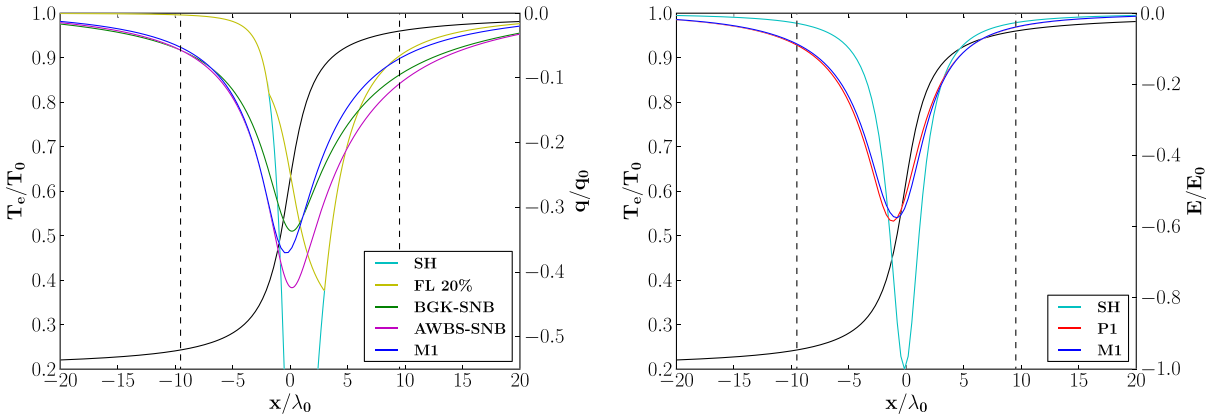

FIG. 1. Analysis of the heat transport on the temperature gradient. (a) Comparison between the different heat flux models. In black, the temperature, in celestial, the SH flux, in yellow, the 20% FL, in green and violet, the SNB models using, respectively, the BGK and the AWBS collision operators, and in blue, the M1 model. The two vertical dashed lines indicate the regions where the kinetic analysis is done. (b) Local electric field spatial distribution compared with the nonlocal one. The first is computed using the SH theory and is used in the SH model and in the diffusive ones (BGK-SNB, AWBS-SNB). The latter is computed using the P1 and the M1 models.

closure relations, Eqs. (15) and (8), respectively. For the electric field, the differences between both closures are negligible.

We proceed to a kinetic description of the system. By using the expressions (13) and (14), we calculate the total EDF in the cold and hot regions of plasma, specified by black dashed vertical lines in Fig. 1.

Figure 2 shows the logarithm of the normalized total EDF for M1 and P1 in the cold and in the hot plasma region. We also show the first moment as a function of velocity in both regions and for both models.

Suprathermal electrons, created in the hot region, travel along their MFP until the cold region, where they deposit their energy. In the hot region, the EDFs are almost isotropic because only a small fraction of electrons is moved away. Since these electrons are very energetic compared to the cold region temperature, they strongly affect the cold EDF, inducing a stronger anisotropy.

Figure 2(a) displays the limit of the P1 model: because of its linear form, a stream of suprathermal electrons, moving from the right to the left ($\theta = 180°$), forces the EDF to become negative for electrons moving in the opposite direction ($\theta = 0°$). This can be better seen in Fig. 3, where we present the anisotropic part of EDF normalized to f_0: $(f_e - f_0)/f_0 = \Delta f_e/f_0$. The P1 model adds an unphysical anisotropy in the opposite direction ($70° < \theta < 250°$).

The differences between the M1 and the P1 models increase if the anisotropy increases ($\delta_{NL} = 0.5\,\mu$m in Eq. (19)), as shown in Fig. 4(a). In this case, SNB models are not able to describe the heat flux because of their local hypothesis on the electric fields, which causes the unphysical modulation of the flux. Differences between P1 and M1 models are stronger in the phase space, as shown in Fig. 4(b).

In summary, the M1 model succeeds in reproducing the nonlocal features: the natural limitation, the preheat in front of the temperature gradient, and it shows a good agreement with the SNB model. Besides that the M1 closure relation, compared to the P1 one, does not modify the flux calculation but at a kinetic level changes some parts of the EDF.

B. Temperature modulation

In this subsection, we compare both modified models in a wide range of nonlocal regimes.

For comparison of the nonlocal transport models, we consider the Epperlein-Short (ES) test.[26] It consists in the study of the flux limitation effect in the electron heat transport, for a plasma with a static temperature modulation

$$T_e(x) = T_0 + T_1 \sin(kx),$$

where k is the wavenumber, $T_0 = 1\,\text{keV}$, and $T_1 = 0.1\,\text{keV}$. The plasma is a fully ionized Beryllium gas of a constant density $4.472 \times 10^{22}\,\text{cm}^{-3}$. Figure 5 shows the heat flux in such a plasma in the case $k\lambda_0 \approx 8 \times 10^{-2}$. In this test, P1 and M1 give the same results, also for EDFs.

Figure 6 shows the complete results of the ES test. The analytical fit obtained from FP simulations is plotted as a function of the nonlocal parameter $k\lambda_0$, in different regimes: $q_{FP}/q_0 = 1/(1 + 50k\lambda_0)$.

The M1 model, as well as the SNB models, agree pretty well with the FP results, except for $k\lambda_0 \approx 1$. This is because M1, as P1, is a model closed at the first moment. Hence, it is able to describe only one direction of anisotropy, while in the ES test there are two opposite directions of anisotropy. When the two opposite beams of fast electrons overlap ($k\lambda_0 \approx 1$), the M1 model is no longer a good approximation. However, when this happens, the heat flux is reduced by a factor greater than 50.

C. Flux rotation and counterstreaming

The M1 model provides also a good estimate for nonlocal fluxes in the two-dimensional geometry. Figure 7 shows with a color bar the temperature profile of a fully ionized Beryllium plasma at a constant density of $4.472 \times 10^{22}\text{cm}^{-3}$. The analytical form of the temperature is

$$T_e(x,y) = T_e(x)\left(\frac{x_{\max}}{2x}\right)^{1/p(y)},$$

where $T_e(x)$ is given by Eq. (19), $p(y) = 3\exp[y^2/(Lx_{\max})]$, $L = 200\,\mu$m, and $x_{max} = 50\,\mu$m is the length of the target along the x axis.

We present here the results obtained with the M1 model. The P1 and SNB models provide very similar results.

In Fig. 7, arrows indicate the local and the M1 heat fluxes. In the nonlocal case, the sharpness of the horizontal gradient influences the vertical flux, inducing a rotation of the latter with respect to the temperature gradient. Cuts along the horizontal and vertical axes are drawn in order to demonstrate

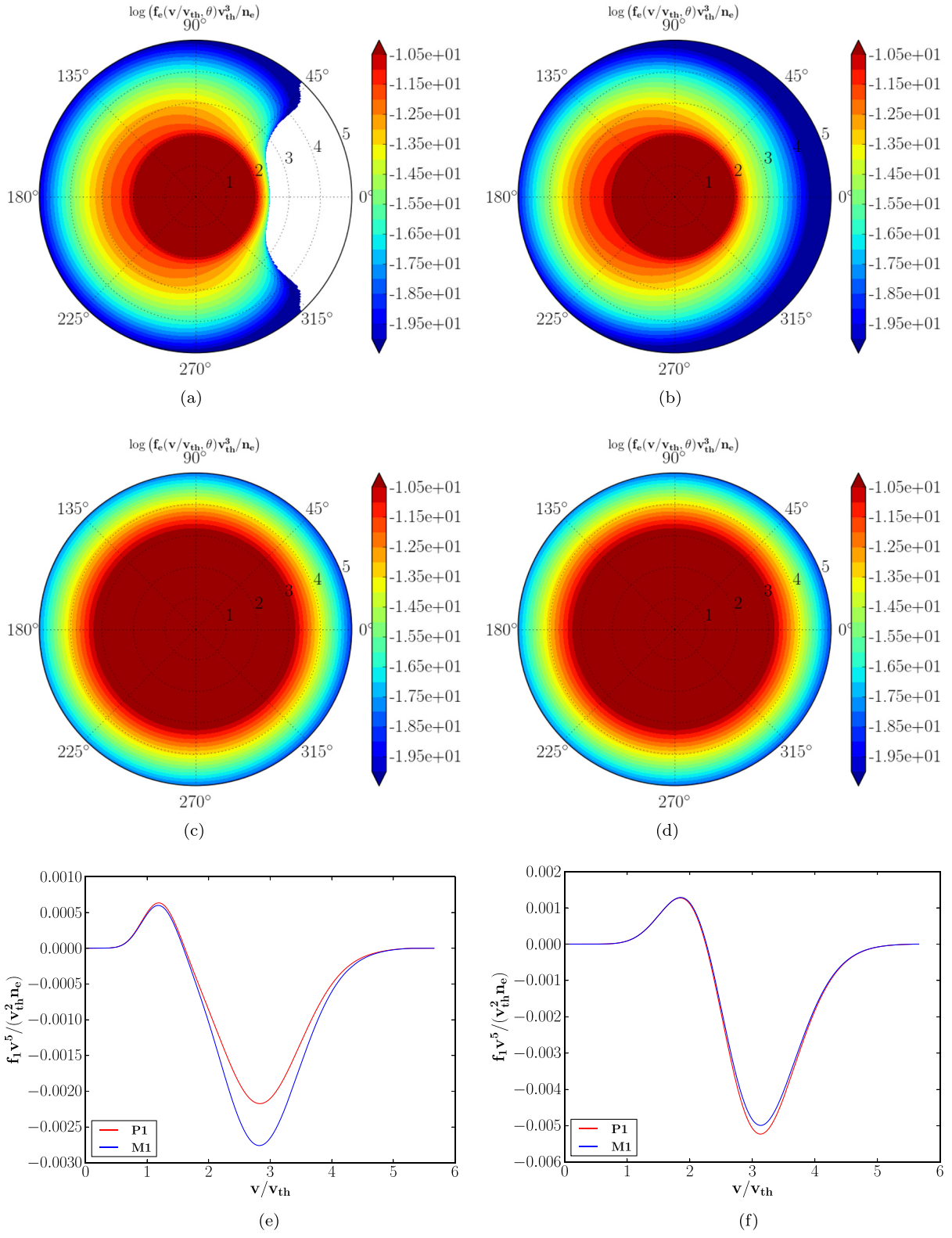

FIG. 2. Analysis of the EDF and its moments in the velocity space. Velocities are shown in the radial direction in polar plots. They are normalized on the thermal velocity while EDF in the hot region v_{th}. The out-of-bord values are uniformly painted with the bord colors. (a) P1, total EDF in the cold (left) region of the plasma. (b) M1, total EDF in the cold region of the plasma. (c) P1, total EDF in the hot (right) region of the plasma. (d) M1, total EDF in the hot region of the plasma. (e) Comparison of the models for the integrand function in the cold region of the plasma. (f) Comparison of the models for the integrand function in the hot region of the plasma.

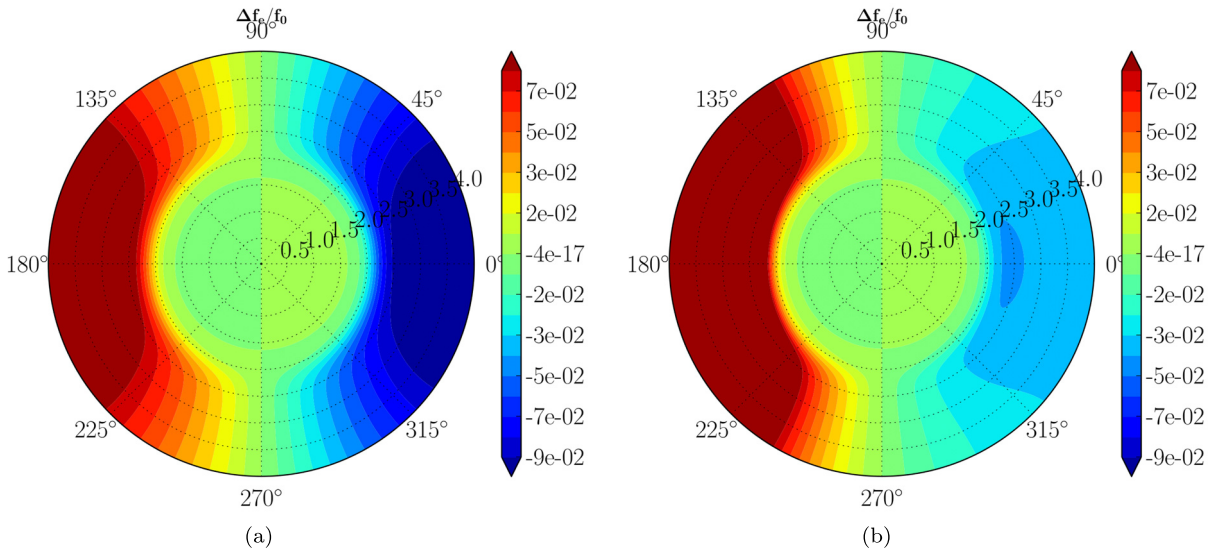

FIG. 3. Anisotropic part of the EDF (defined as $\Delta f_e/f_0 = f_e/f_0 - 1$) in the cold region of plasma (shown in Fig. 1(a)), as a function of the velocity, normalized by the thermal velocity in the hot region. (a) P1 description. (b) M1 description.

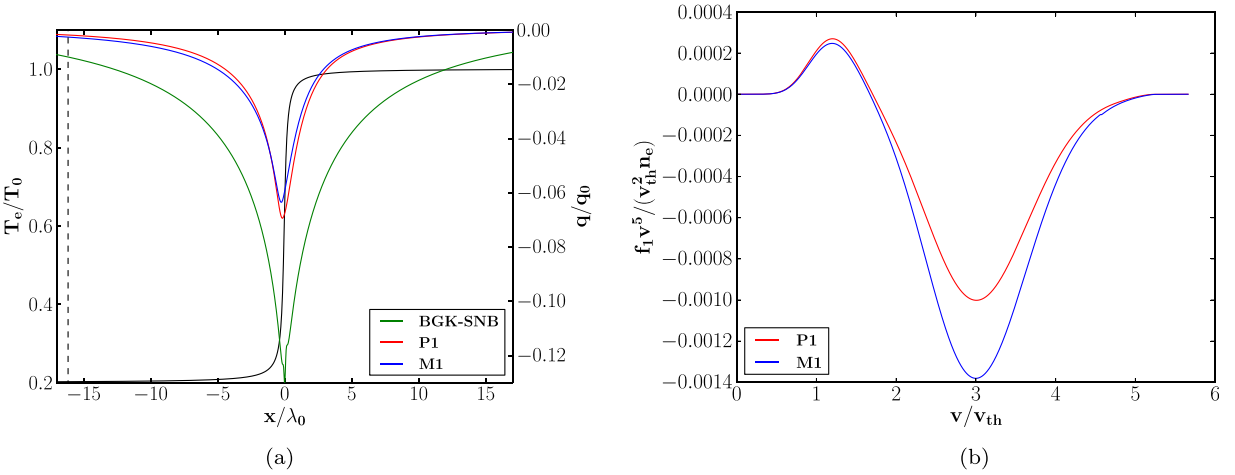

FIG. 4. Comparison of transport models for the heat flux analysis in the case of a sharp temperature gradient. (a) Heat fluxes for different models. The vertical dashed line represents the place where the EDF is shown in panel 4(b) ($-16\lambda_0$). (b) Integrand function of the heat flux, as a function of velocity for the two advective models.

the differences. In Fig. 8(a), the horizontal cut shows the main flux, induced by the sharpest gradient. We also see a counterstreaming flux, which has the opposite sign with respect to the local one. This effect can also be seen in monodimensional simulations. Figure 8(b) presents two M1 fluxes. The continuous blue line is the vertical cut of Fig. 7, while the dashed blue one is the result of a monodimensional simulation with the same vertical temperature gradient. This allows to see how the horizontal gradient affects the vertical one.

The M1 model is also able to reproduce the main multidimensional nonlocal feature: the flux rotation to a competition between the counterstreaming flux and to the crossed interaction.

V. NONLOCAL LANDAU DAMPING

In Section IV, we have shown that the M1 model is able to describe complete EDFs, contrarily to the P1 model, which

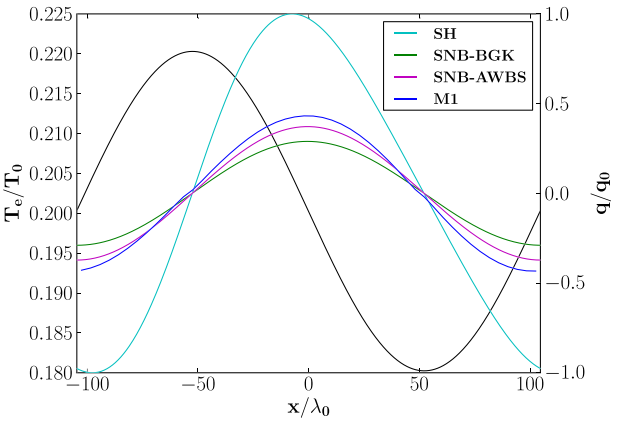

FIG. 5. Study of the heat flux for a modulated temperature, using the local model, the SNB ones and M1. P1 results are not shown because very similar to M1, black line shows the temperature modulation. Periodic boundary conditions are applied.

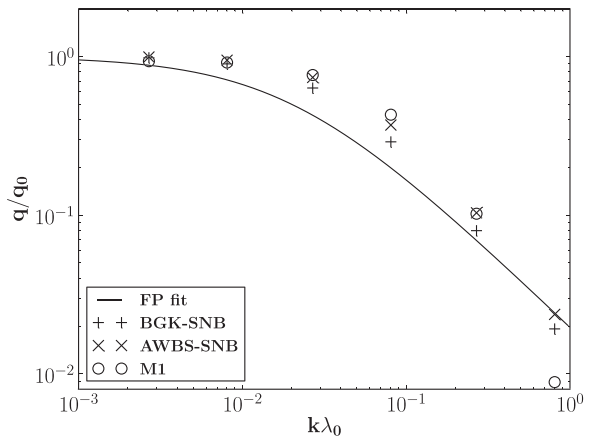

FIG. 6. Heat flux limitation in the ES test. Solid line presents the FP fit, for a sinusoidal modulation of temperature. The results are given in function of the wavenumber normalized with the MFP.

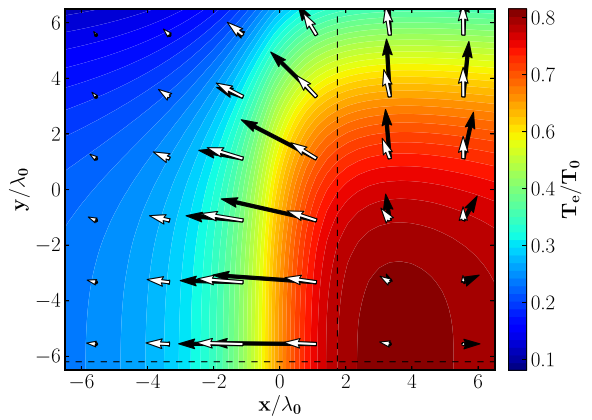

FIG. 7. Two dimensional analysis of the heat transport. The color background traces the temperature. Arrows describe the magnitude and direction of heat fluxes. The SH model, in black, is compared with M1, in white. Dashed black lines denote the cuts shown in Fig. 8.

may lead to negative (unphysical) values. Besides heat transport, this property allows the kinetic description of a wide range of collective phenomena. Here, we focus on the study of the Landau damping[27] of longitudinal plasma waves: the Langmuir and the ion-acoustic waves,[28,29] in the nonlocal case of a steep temperature gradient considered in Section IV A.

A. Langmuir waves

The Langmuir waves are high-frequency electron oscillations corresponding to the electric field perturbations on a microscopic scale. A modification of the EDF in the heat transport zone may strongly affect the stability of Langmuir waves, especially downstream the temperature jump. Since this phenomenon is not related to collisions, in a first step we neglect them, for the sake of simplicity.

A dispersion equation for the longitudinal waves corresponds to zeros of the longitudinal dielectric permittivity $\epsilon^l(\omega,k)=0$. Because of their inertia, ions do not play a role in Langmuir waves and the dielectric permittivity reads[19,27]

$$\epsilon^l(\omega,k)=1+\delta\epsilon_e^l=1+\frac{4\pi e^2}{k^2 m_e}\int_{\mathbf{R}^3}\frac{d^3v}{\omega-\vec{k}\cdot\vec{v}}\vec{k}\cdot\frac{\partial}{\partial\vec{v}}f_e(\vec{v}). \tag{20}$$

The temporal evolution of the wave amplitude depends on the imaginary part of the dielectric permittivity. Depending on its sign, it leads to a wave damping or an instability. In the linear damping theory, the imaginary term is assumed to be small, compared to the real one. Defining the damping rate as $\gamma=-\Im(\omega)$, we have $\omega=\Re(\omega)-i\gamma$ where the damping rate reads

$$\gamma=\frac{\Im(\epsilon^l)}{\frac{\partial}{\partial\omega}\Re(\epsilon^l)}. \tag{21}$$

According to the general approach,[19,27] the dielectric permittivity is calculated by separating the denominator in Eq. (20) in the principal value and the pole

$$\frac{1}{\omega-\vec{k}\cdot\vec{v}}=\frac{P}{\omega-\vec{k}\cdot\vec{v}}-i\pi\delta(\omega-\vec{k}\cdot\vec{v}),$$

where P stands for principal value.

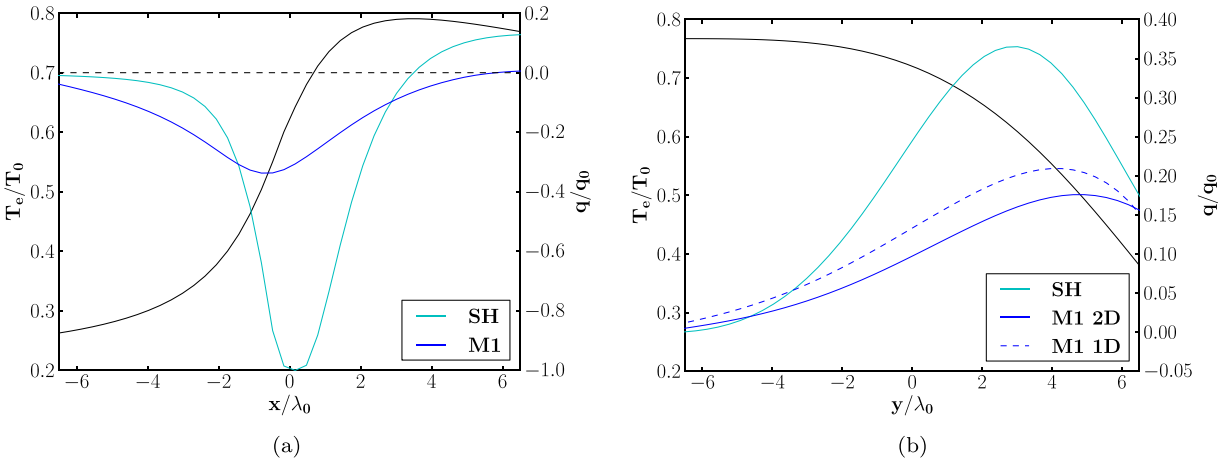

FIG. 8. Cuts of the fluxes of Fig. 7. (a) Horizontal cut. The dashed horizontal line indicates the zero flux. (b) Vertical cut. The dashed blue line describes a monodimensional simulation using the same vertical gradient.

In the Cartesian coordinate system, the damping rate goes like

$$\gamma \propto -\left[v_{\parallel} \frac{\partial F_{\parallel}(v_{\parallel})}{\partial v_{\parallel}} \right]_{v_{\parallel}=\omega/k}, \tag{22}$$

where $F_{\parallel}(v_{\parallel}) = \int d^2 v_{\perp} f_e$ and the symbols $\parallel$ and $\perp$ mean, respectively, the parallel and the perpendicular directions with respect to the wavevector $\vec{k}$. Figure 9 shows the typical case where Langmuir wave instabilities develop. A positive gradient is induced by a population of hot electrons, which are transported to the cold region of plasma from the hot one. As our models are based on a spherical coordinate description of EDF, expressions for the damping rate are more complicated. The integrals in Eq. (20) are calculated in the spherical coordinate system with the vector $\vec{k}$ parallel to the temperature gradient: $\vec{k} \cdot \vec{v} = kv\mu$. The M1 EDF is given by Eq. (14). Developing the denominator to the third order for the parameter $kv\mu/\omega \ll 1$, the real part of dielectric permittivity is

$$\Re\left(\delta\epsilon_e^l\right) = -\left(\frac{\omega_{pe}}{\omega}\right)^2 \frac{1}{n_e} \left\{ \int_{\mathbf{R}} dv v^2 f_0 + 2\frac{k}{\omega} \int_{\mathbf{R}} dv v^3 f_0 I_1 + 3\left(\frac{k}{\omega}\right)^2 \int_{\mathbf{R}} dv v^4 f_0 I_2 \right\}, \tag{23}$$

where $\omega_{pe} = \sqrt{4\pi e^2 n_e / m_e}$ is the electron plasma frequency and

$$\begin{cases} I_1 = \coth(\alpha_1) - \alpha_1^{-1} \\ I_2 = 1 - 2\alpha_1^{-1}\coth(\alpha_1) - 2\alpha_1^{-2}. \end{cases}$$

The imaginary part reads

$$\Im\left(\delta\epsilon_e^l\right) = \frac{\omega_{pe}^2 \pi}{2 n_e k^2} \left\{ \frac{\omega}{k} \frac{f_0\left(\frac{\omega}{k}\right)\alpha_1\left(\frac{\omega}{k}\right)}{\sinh\left[\alpha_1\left(\frac{\omega}{k}\right)\right]} e^{\alpha_1\left(\frac{\omega}{k}\right)} - \int_{\frac{\omega}{k}}^{\infty} dv \frac{f_0 \alpha_1^2}{\sinh(\alpha_1)} e^{\frac{\alpha_1 \omega}{kv}} \right\},$$

so the damping rate is

$$\frac{\gamma}{\omega} = \left(\frac{\omega}{k}\right)^2 \frac{\pi}{4} \frac{\frac{\omega}{k} \frac{f_0\left(\frac{\omega}{k}\right)\alpha_1\left(\frac{\omega}{k}\right)}{\sinh\left[\alpha_1\left(\frac{\omega}{k}\right)\right]} e^{\alpha_1\left(\frac{\omega}{k}\right)} - \int_{\frac{\omega}{k}}^{\infty} dv \frac{f_0 \alpha_1^2}{\sinh(\alpha_1)} e^{\frac{\alpha_1 \omega}{kv}}}{\int_{\mathbf{R}} dv v^2 f_0 + 3\frac{k}{\omega} \int_{\mathbf{R}} dv v^3 f_0 I_1 + 6\left(\frac{k}{\omega}\right)^2 \int_{\mathbf{R}} dv v^4 f_0 I_2}. \tag{24}$$

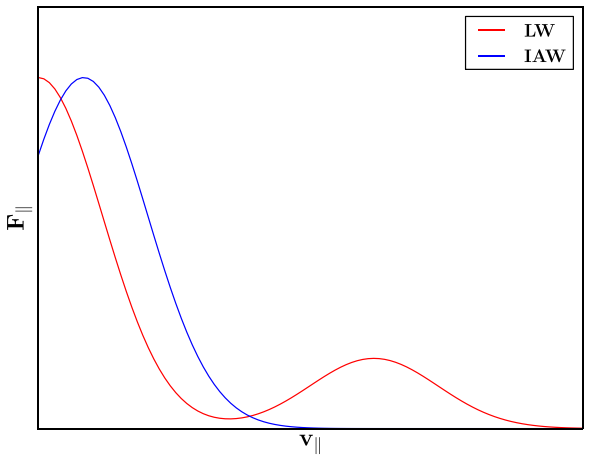

FIG. 9. EDFs integrated over perpendicular velocity, as functions of the parallel velocity, in typical cases of instability development for Langmuir waves (LW) and for ion-acoustic waves (IAW).

The P1 damping rate is obtained from Eq. (24), in the linear limit for $\alpha_1 \approx 3f_1/f_0 \ll 1$

$$\frac{\gamma}{\omega} = \left(\frac{\omega}{k}\right)^2 \frac{\pi}{4} \frac{\frac{\omega}{k} f_0\left(\frac{\omega}{k}\right) + 3\frac{\omega}{k} f_1\left(\frac{\omega}{k}\right) - 3\int_{\frac{\omega}{k}}^{\infty} dv f_1}{\int_{\mathbf{R}} dv v^2 f_0 + 2\frac{k}{\omega}\int_{\mathbf{R}} dv v^3 f_1 + 3\left(\frac{k}{\omega}\right)^2 \int_{\mathbf{R}} dv v^4 f_0}. \tag{25}$$

This relation can also be obtained by considering the EDF in Eq. (8).

The real part of the Langmuir wave frequency is not affected by the transport effects and it is given by the standard Bohm-Gross relation, $\Re(\omega) \approx \pm\omega_{pe}[1 + (3/2)k^2\lambda_{De}^2]$. Here, $\lambda_{De} = v_{th}/\omega_{pe}$ is the local Debye length.

We consider the heat transport along the temperature gradient for the cold EDFs shown in Fig. 2. The Langmuir wave damping rate is shown in Fig. 10 as a function of the wavenumber, for waves propagating forward and backward with respect to the temperature gradient. The models shown are the hydrodynamic one (HD), P1, and M1. The damping rate for the HD model is given by Eq. (25), with $f_0 = f_0^m$ and $\vec{f}_1 = 0$. Figure 10 shows that hot electrons disturb Langmuir waves, inducing instability in the direction of hot electron propagation (backward waves), for wavenumbers $k\lambda_{De} \approx 0.15 - 0.25$. The differences between the two nonlocal models are both quantitative and qualitative: damping rates are different but also may have different signs, depending on the wavenumber. Moreover, the P1 model produces a spurious instability in the forward direction because it transforms an unphysical behavior (negative total EDF) into an instability, as shown in Fig. 10(a).

Collisions can be accounted for in the damping of Langmuir waves by adding an additional term in the imaginary part of the electron dielectric permittivity, $\Im(\delta\epsilon_e^l) = \omega_{pe}^2 \nu_{eff}/\omega^3$, where

$$\nu_{eff} = \frac{4\sqrt{2\pi}}{3} \frac{Z^2 e^4 n_i \Lambda_{ei}}{m_e^2 v_{th}^3}$$

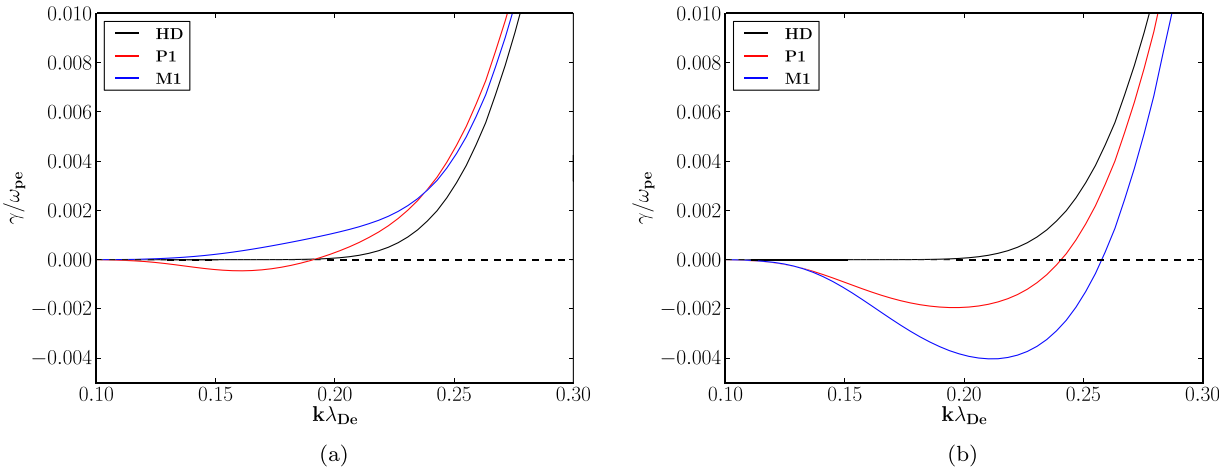

FIG. 10. Damping rate of Langmuir waves, normalized to the electron plasma frequency, as a function of the wavenumber normalized to the local Debye length, for the hydrodynamic theory (HD), and for M1 and P1. (a) Forward wave propagation. (b) Backward wave propagation.

is the effective collision frequency.[19] This term is the same for all models and corresponds to the collision term $-\nu_{eff}\delta f$ in the FP equation.

The results for the collisional Landau damping of Langmuir waves, for the downstream temperature zone in Fig. 2, are shown in Fig. 11. We see that the instability rate is reduced and the unphysical unstability for the forward propagating wave disappears. However, the difference between the models is evident: while the instability disappears for P1, it is still present for the M1 model. The expected growth rate $\gamma \sim 5 \times 10^{13}\,\mathrm{s}^{-1}$ corresponds to a time much shorter than the typical hydrodynamic time. Therefore, one may expect that the Langmuir turbulence can be developed downstream the temperature gradient, possibly affecting the electron heat flux.

B. Ion-acoustic waves

The ion-acoustic waves are low-frequency waves ($\omega/k \ll v_{th}$) which involve electrons and ions. Similar to the Langmuir waves, the spectrum of ion-acoustic waves is defined by zeros of the dispersion equation $\epsilon^l(\omega,k)=0$, where $\epsilon^l = 1+\delta\epsilon_e^l+\delta\epsilon_i^l$ includes the electron and the ion contribution. In calculation of the ion dielectric permittivity, we assume the ions to be cold, $\delta\epsilon_i^l \approx -\omega_{pi}^2/\omega^2$, where $\omega_{pi} = \sqrt{4\pi Ze^2 n_i/m_i}$ is the ion plasma frequency.

Calculating the electron dielectric permittivity, defined by (20), in the low frequency limit $\omega \ll kv_{th}$, we obtain the following expression in the spherical coordinates:

$$\Re\left(\delta\epsilon_e^l\right) = \frac{\omega_{pe}^2}{k^2}\frac{1}{n_e}\left\{\int_{\mathbf{R}} dv f_0 - \int_{\mathbf{R}} dv f_0\left[\frac{\alpha_1^2\Xi(\alpha_1)}{\sinh(\alpha_1)} - \alpha_1\coth(\alpha_1)+1\right]\right\},$$

where

$$\Xi(x) = \int_0^x dy \frac{\sinh(y)}{y}.$$

In the limit $\alpha_1 \ll 1$, the electron contribution reduces to $\Re(\delta\epsilon_e^l) = 1/(k^2\lambda_{De}^2)$. Correspondingly, the expression for the ion-acoustic wave frequency reads

$$\omega^2 = \frac{\omega_{pi}^2 k^2\lambda_{De}^2}{1+k^2\lambda_{De}^2},$$

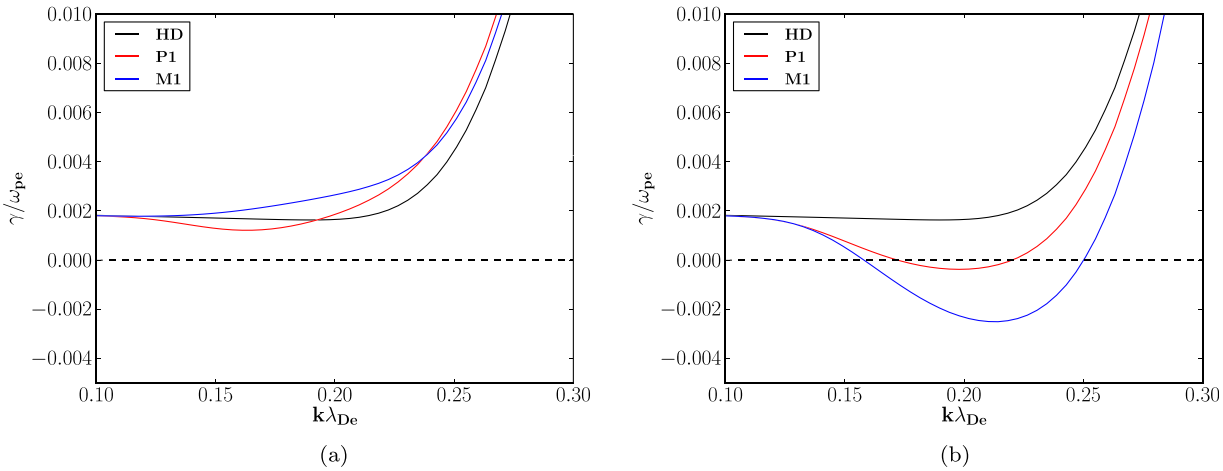

FIG. 11. Damping rate of Langmuir waves, accounting for the collision term. (a) Forward wave propagation. (b) Backward wave propagation.

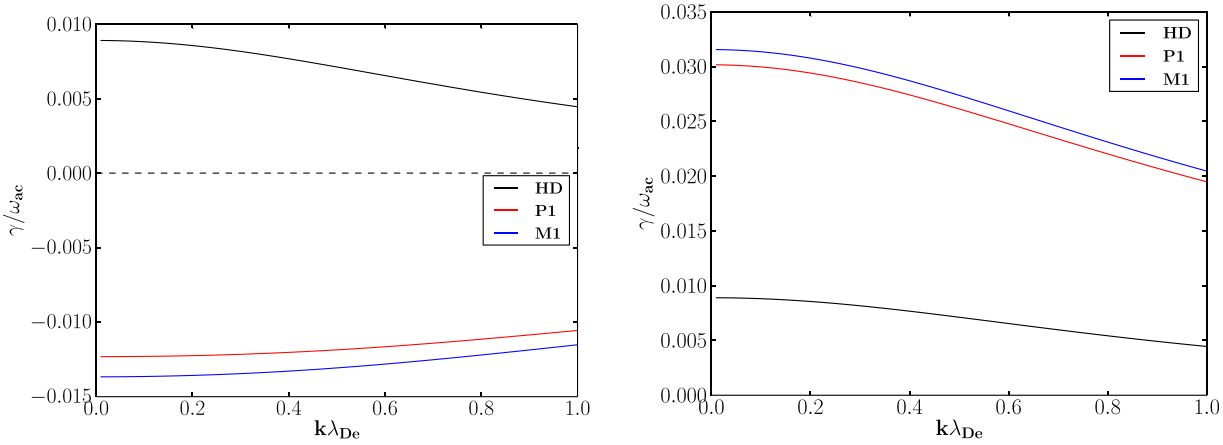

FIG. 12. Damping rate of ion-acoustic waves, normalized to the ion acoustic frequency $\omega_{ac} = kc_s$, as a function of the wavenumber normalized with the local Debye length. (a) Forward wave propagation. (b) Backward wave propagation.

where $\omega_{pi}\lambda_{De} = c_s$ is the local sound speed.

The general expression (21) also applies to the ion-acoustic wave damping. Following the procedure described for Langmuir waves (see also Ref. 28), the damping rate of the ion-acoustic waves reads

$$\frac{\gamma}{\omega} = \frac{\pi}{4}\frac{\frac{\omega}{k}\frac{f_0\left(\frac{\omega}{k}\right)\alpha_1\left(\frac{\omega}{k}\right)}{\sinh\left[\alpha_1\left(\frac{\omega}{k}\right)\right]}e^{\alpha_1\left(\frac{\omega}{k}\right)} - \int_{\frac{\omega}{k}}^{\infty} dv\,\frac{f_0\alpha_1^2}{\sinh(\alpha_1)}e^{\frac{\alpha_1\omega}{kv}}}{\int_{\mathbf{R}} dv f_0 - \int_{\mathbf{R}} dv f_0\left[\frac{\alpha_1^2\Xi(\alpha_1)}{\sinh(\alpha_1)} - \alpha_1\coth(\alpha_1) + 1\right]}.$$

This expression simplifies in the linear limit in α_1, which corresponds to the P1 model

$$\frac{\gamma}{\omega} = \frac{\pi}{4}\frac{\frac{\omega}{k}f_0\left(\frac{\omega}{k}\right) + 3\frac{\omega}{k}f_1\left(\frac{\omega}{k}\right) - 3\int_{\frac{\omega}{k}}^{\infty} dv f_1}{\int_{\mathbf{R}} dv f_0}.$$

An example of the ion-acoustic wave damping is shown in Fig. 12 (forward and backward propagating waves), for the position $x = 0$ in Fig. 1(b). The damping is strongly modified near the maximum of the temperature gradient. The ion-acoustic waves propagating in the forward direction become unstable, while the waves propagating in the backward direction are stronger damped.

This ion-acoustic instability is induced by the return current, as it has been explained in Ref. 28. In Fig. 9, it is schematically illustrated that the positive derivative of $F(v_\parallel)$ is induced by the shift of the maximum of the EDF due to the electric field, which induces the return current.

The instability is obtained for both models; however, the location of the instability can be different because the difference of location of the electric field maximum, as shown in Fig. 1(b). The small differences between M1 and P1 models are explained by the fact that the ion-acoustic waves have very low phase velocities and the details of the EDF at high velocities do not have large importance.

For the plasma parameters presented in Fig. 1, the ion plasma frequency is of the order of $10^{14}\,\mathrm{s}^{-1}$ and the ion-acoustic instability can be excited in a few picosecond time scale. It could introduce an effective (turbulent) resistivity and suppress the heat transport.[30]

VI. CONCLUSIONS

In this paper, we have presented a new nonlocal model of electron energy transport in high-energy-density plasmas, based on the kinetic FP equation and on an entropic closure relation. This model has been compared with two SNB models, using different collision operators and with the P1 model, in different conditions of heat transport. The M1 model reproduces all nonlocal features in one and two spatial dimensions and gives a better description of the EDF. This provides access to small scale collective phenomena such as Landau damping of Langmuir and ion-acoustic waves. It is shown that in front of the temperature gradient and around the maximum of the temperature gradient, the Langmuir and the ion-acoustic instabilities may be developed, thus reducing the MFP of the electrons and consequently affecting the nonlocality of the flux.

The structure of the M1 model allows to naturally take into account electromagnetic fields, which is also a crucial issue for the high-energy-density physics applications.

ACKNOWLEDGMENTS

The authors are grateful to Jérôme Breil, Arnaud Colaïtis, and Rachel Nuter for discussions and numerical support. This work has been carried out within the framework of the EUROfusion Consortium and has received funding from the European Unions Horizon 2020 research and innovation programme under Grant Agreement No. 633053.

[1]V. N. Goncharov, O. V. Gotchev, E. Vianello, T. R. Boehly, J. P. Knauer, P. W. McKenty, P. B. Radha, S. P. Regan, T. C. Sangster, S. Skupsky, V. A. Smalyuk, R. Betti, R. L. McCrory, D. D. Meyerhofer, and C. Cherfils-Cleroin, "Early stage of implosion in inertial confinement fusion: shock timing and perturbation evolution," Phys. Plasmas **13**(1), 012702 (2006).

[2]L. Spitzer and R. Härm, "Transport phenomena in a completely ionized gas," Phys. Rev. **89**(5), 977 (1953).

[3]R. C. Malone, R. L. McCrory, and R. L. Morse, "Indications of strongly flux-limited electron thermal conduction in laser-target experiments," Phys. Rev. Lett. **34**(12), 721 (1975).
[4]J. F. Luciani, P. Mora, and J. Virmont, "Nonlocal heat transport due to steep temperature gradients," Phys. Rev. Lett. **51**(18), 1664 (1983).
[5]J. R. Albritton, E. A. Williams, I. B. Bernstein, and K. P. Swartz, "Nonlocal electron heat transport by not quite Maxwell-Boltzmann distributions," Phys. Rev. Lett. **57**(15), 1887 (1986).
[6]W. Manheimer, D. Colombant, and V. Goncharov, "The development of a Krook model for nonlocal transport in laser produced plasmas. I. Basic theory," Phys. Plasmas **15**(8), 083103 (2008).
[7]A. Bendib, J. F. Luciani, and J. P. Matte, "An improvement of the nonlocal heat flux formula," Phys. Fluids **31**(4), 711–713 (1988).
[8]S. I. Krasheninnikov, "On nonlocal electron heat conduction," Phys. Fluids B: Plasma Phys. **5**(1), 74–76 (1993).
[9]A. Marocchino, M. Tzoufras, S. Atzeni, Ph. Schiavi, A. Nicolaï, J. Mallet, V. Tikhonchuk, and J.-L. Feugeas, "Comparison for non-local hydrodynamic thermal conduction models," Phys. Plasmas **20**(2), 022702 (2013).
[10]A. V. Brantov and V. Yu. Bychenkov, "Nonlocal transport in hot plasma. Part I," Plasma Phys. Rep. **39**(9), 698–744 (2013).
[11]G. P. Schurtz, Ph. Nicolaï, and M. Busquet, "A nonlocal electron conduction model for multidimensional radiation hydrodynamics codes," Phys. Plasmas **7**(10), 4238–4249 (2000).
[12]J.-L. Feugeas, Ph. Nicolai, X. Ribeyre, G. Schurtz, V. Tikhonchuk, and M. Grech, "Modeling of two-dimensional effects in hot spot relaxation in laser-produced plasmas," Phys. Plasmas **15**(6), 062701 (2008).
[13]A. Marocchino, S. Atzeni, and A. Schiavi, "Effects of non-local electron transport in one-dimensional and two-dimensional simulations of shock-ignited inertial confinement fusion targets," Phys. Plasmas **21**(1), 012701 (2014).
[14]Ph. Nicolaï, J.-L. Feugeas, and G. P. Schurtz, "A practical nonlocal model for heat transport in magnetized laser plasmas," Phys. Plasmas **13**(3), 032701 (2006).
[15]R. J. Kingham and A. R. Bell, "Nonlocal magnetic-field generation in plasmas without density gradients," Phys. Rev. Lett. **88**(4), 045004 (2002).
[16]G. N. Minerbo, "Maximum entropy Eddington factors," J. Quant. Spectrosc. Radiat. Transfer **20**(6), 541–545 (1978).
[17]B. Dubroca, J.-L. Feugeas, and M. Frank, "Angular moment model for the Fokker-Planck equation," Eur. Phys. J. D **60**(2), 301–307 (2010).
[18]M. Touati, J. L. Feugeas, Ph. Nicolaï, J. J. Santos, L. Gremillet, and V. T. Tikhonchuk, "A reduced model for relativistic electron beam transport in solids and dense plasmas," New J. Phys. **16**(7), 073014 (2014).
[19]L. D. Landau and E. M. Lifshitz, *Physical Kinetics* (Robert Maxwell, M.C., 1981).
[20]I. P. Shkarofsky, T. W. Johnston, and M. P. Bachynski, *The Particle Kinetics of Plasmas* (McGraw-Hill, 1973).
[21]N. A. Krall and A. W. Trivelpiece, *Principles of Plasma Physics* (Addison-Wesley, 1966).
[22]J. R. Albritton, "Laser absorption and heat transport by non-Maxwell-Boltzmann electron distributions," Phys. Rev. Lett. **50**(26), 2078 (1983).
[23]J. P. Matte and J. Virmont, "Electron heat transport down steep temperature gradients," Phys. Rev. Lett. **49**(26), 1936 (1982).
[24]B. Dubroca and J.-L. Feugeas, "Etude théorique et numérique d'une hiérarchie de modèles aux moments pour le transfert radiatif," C.R. Acad. Sci., Ser. I-Math. **329**(10), 915–920 (1999), available at http://www.sciencedirect.com/science/article/pii/S0764444200874996.
[25]P. L. Bhatnagar, E. P. Gross, and M. Krook, "A model for collision processes in gases. I. Small amplitude processes in charged and neutral one-component systems," Phys. Rev. **94**(3), 511 (1954).
[26]E. M. Epperlein and R. W. Short, "A practical nonlocal model for electron heat transport in laser plasmas," Phys. Fluids B: Plasma Phys. **3**(11), 3092–3098 (1991).
[27]R. J. Goldston and P. H. Rutherford, *Introduction to Plasma Physics* (Institute of Physics Publishing, 1995).
[28]V. T. Tikhonchuk, W. Rozmus, V. Yu. Bychenkov, C. E. Capjack, and E. Epperlein, "Return current instability in laser heated plasmas," Phys. Plasmas **2**(11), 4169–4173 (1995).
[29]A. V. Brantov, V. Yu. Bychenkov, and W. Rozmus, "Ion acoustic instability driven by a temperature gradient in laser-produced plasmas," Phys. Plasmas **8**(8), 3558–3564 (2001).
[30]W. Rozmus, V. T. Tikhonchuk, V. Yu. Bychenkov, and C. E. Capjack, "Enhanced ion acoustic fluctuations in laser-produced plasmas," Phys. Rev. E **50**(5), 4005 (1994).